JOURNAL OF GEOPHYSICAL RESEARCH, VOL. 111, A11S15, doi:10.1029/2006JA011620, 2006



# Magnetically self-consistent ring current simulations during the 19 October 1998 storm

Margaret W. Chen,[1] Shuxiang Liu,[2] Michael Schulz,[3] James L. Roeder,[1] and Larry R. Lyons[2]

Received 16 January 2006; revised 12 September 2006; accepted 9 October 2006; published 23 November 2006.

[1] We investigate effects of magnetic self-consistency on ring current development by calculating equatorial particle transport in a model that feeds back the ring current on the magnetospheric configuration. The equatorial magnetic intensity is computed by solving a force-balance equation in the equatorial plane. This force-balance computation is coupled to a kinetic proton and electron drift-loss model. The electric field model used includes corotation, quiescent Volland-Stern convection, and storm-associated enhancements in the convection. We have modeled the 19 October 1998 storm (min $Dst = -112$ nT) by using the total cross polar cap potential from AMIE to determine the amplitudes of storm-associated electric field enhancements. We trace equatorially mirroring protons and electrons within this model. We have found that self-consistent feedback between plasma pressure and the magnetic field tends to mitigate the energization associated with inward particle transport as the ring current forms. At a given first adiabatic invariant and radial distance, the self-consistent magnetic field reduces the $\mathbf{E} \times \mathbf{B}$ drift rate as it significantly enhances the azimuthal gradient-$\mathbf{B}$ drift rate. Especially later in the main phase, there can be places where the plasma pressure and magnetic perturbation are locally enhanced by making the simulation magnetically self-consistent because of enhanced drift rates in regions of reduced magnetic intensity. The southward magnetic perturbation at the center of the Earth, which represents the ring current contribution to the *Dst* index, is reduced by about 25% by making the simulation magnetically self-consistent. This suggests that simulations that do not take account of the feedback of the ring current overestimate the actual ring current intensity.

**Citation:** Chen, M. W., S. Liu, M. Schulz, J. L. Roeder, and L. R. Lyons (2006), Magnetically self-consistent ring current simulations during the 19 October 1998 storm, *J. Geophys. Res.*, *111*, A11S15, doi:10.1029/2006JA011620.

## 1. Introduction

[2] An important consequence of the storm time ring current is that it perturbs the geomagnetic field. This magnetic perturbation is thought to contribute significantly to the widely used *Dst* index, which is measured by the longitude-averaged magnetic field perturbation at low-latitudes on the surface of the Earth. Historically, the *Dst* index has been regarded as a direct measure of ring current strength. More recently it has been recognized that other current systems such as the dayside magnetopause currents and nightside tail currents [*Turner et al.*, 2000] also contribute importantly to *Dst*. Even so, large magnetic field depressions ($\sim -100$ to $-200$ nT) due to the ring current itself have been measured in situ at $L \sim 3$–$4$ during storms [e.g., *Cahill*, 1969; *Wygant et al.*, 1998]. Several recent statistical analyses involving large databases of in situ magnetic field measurements in the inner magnetosphere [*Tsyganenko et al.*, 2003; *Lui*, 2003; *Ostapenko and Maltsev*, 2003; *Le et al.*, 2004; *Jorgensen et al.*, 2004] have revealed large ($\sim -100$ nT to $-400$ nT) and azimuthally asymmetric depressions in the magnetic field intensity under disturbed conditions. These depressions are thought to be associated with the ring current.

[3] We [*Chen et al.*, 2005] have previously calculated the disturbed magnetic field from simulations of the storm time ring current and have found that the magnetic field disturbance can be especially large in localized regions. For example, at $L \sim 3$–$5$ the magnetic field perturbation was ~70% of the dipole-field value. Similarly, *Zaharia et al.* [2005] have found that large magnetic depressions can form in the inner magnetosphere during storms from their three-dimensional (3-D) modeling. Although these calculations were not done self-consistently, it demonstrated the need for calculating inner magnetospheric particle transport within a magnetospheric magnetic field model that takes consistent account of ring current magnetic field perturbations. As a first step toward a magnetically self-consistent model, we

[1] Space Sciences Applications Laboratory, The Aerospace Corporation, El Segundo, California, USA.
[2] Department of Atmospheric Sciences, University of California, Los Angeles, California, USA.
[3] Lockheed Martin Advanced Technology Center, Palo Alto, California, USA.


0148-0227/06/2006JA011620$09.00

recently developed such a simulation model that takes account of the feedback of the ring current within a magnetic field model that is in force balance with the plasma pressure in the equatorial plane. *Liu et al.* [2006], who reported initial simulation results of this model for a hypothetical storm, found that the magnetically self-consistent model reasonably reproduced many of the general features of the storm time ring current of statistical observational studies [*Terada et al.*, 1998; *Le et al.*, 2004; *Jorgensen et al.*, 2004]. For example, the simulated disturbed magnetic field was as large as $-150$ nT near an equatorial radial distance $r_0$ of 3 $R_E$ and the inner eastward flowing (dominated by magnetization currents) and the main westward flowing ring current were at $r_0 \sim 3$ $R_E$ and $r_0 \sim 4-6.6$ $R_E$, respectively. We found that taking account of the feedback of the ring current tended to mitigate the energization of ring current particles. This was generally consistent with the findings of *Lemon et al.* [2004], who used the Rice Convection Model RCM-E, which consistently accounts for inner magnetospheric currents in calculating the magnetospheric **B**-field configuration, while also coupling these currents with ionospheric currents.

[4] In this paper we use our magnetically self-consistent ring current model to simulate the 19 October 1998 storm, selected to be one of the National Science Foundation (NSF) Geospace Environment Modeling (GEM) Inner Magnetosphere/Storms Assessment Challenge (IMS) events. A nice feature of this storm was that the solar wind pressure was low throughout the main phase so that the decrease in *Dst* was most likely due largely to the ring current rather than decompression. We focus on how taking account of the feedback of the ring current affects distributions of the equatorial perpendicular particle pressure during the main phase of the storm by comparing simulations results with and without the feedback of the ring current. Additionally, we compare the simulated ion differential energy flux profiles with those inferred from Polar/Charge and Mass Magnetospheric Ion Composition Experiment (CAMMICE) measurements. The results of the study elucidate the importance of taking account the feedback of the ring current in studying particle transport in the inner magnetosphere during storms.

## 2. Simulation Model

### 2.1. Magnetic Field Model in Force Balance

[5] In our model we treat magnetic field lines as contours of constant $L$ and azimuthal angle $\phi$, satisfying the equation

$$r = La\left[1 + 0.5(r/b)^3\right]\sin^2\theta, \tag{1}$$

where $r$ is the distance from the point dipole, $a$ (= 1 $R_E$) is the radius of Earth, and $\theta$ is the co-latitude measured from Earth's dipole axis. Equation (1) describes field lines within a magnetic field constructed by superimposing a dipole with a southward magnetic field [*Dungey*, 1961, 1963]. In our past work [e.g., *Chen et al.*, 1994] the parameter $b$ in (1) had been regarded as a constant (equal to the radius of an equatorial neutral line). Now we allow $b$ to vary with $\phi$ and with $L$ (or equivalently with $r_0$) so as to simulate the magnetic effects of an azimuthal ring current. The values of $b$, which represent how much the field line is stretched relative to a dipole, are determined by the equatorial magnetic intensity $B_0$. We assume that each magnetic field line always lies in the same meridian plane (i.e., no field line twisting). This assumption is reasonable within the inner magnetosphere where azimuthal perturbations of the magnetic field due to field-aligned currents and the Chapman-Ferraro current are small compared to the ambient magnetic field. This simplifying approximation is better on the nightside (where we introduce our hot plasma) than on the dayside (where it mostly escapes) because there is more room in latitude to fit field lines inside the magnetosphere when they emerge from dayside footpoints than from nightside foodpoints [*Mead*, 1964; *Schulz and McNab*, 1996]. The equatorial magnetic intensity $B_0$ is computed by solving in the equatorial plane the force balance equation,

$$\mathbf{j} \times \mathbf{B} = \nabla P_\perp + (P_\parallel - P_\perp)\frac{(\mathbf{B}\cdot\nabla)\mathbf{B}}{B^2} \tag{2}$$

where $\mathbf{j} = (\nabla \times \mathbf{B})/\mu_0$ is the current density, $\mu_0$ is the permeability of free space, $P_\perp$ is the perpendicular pressure, and $P_\parallel$ is the parallel pressure. The azimuthal component can be solved analytically (see *Liu et al.* [2006] for algebraic details) and yields

$$B_0^2/2\mu_0 + P_{\perp 0} = P_0^*(r_0), \tag{3}$$

where $P_0^*(r_0)$ is a function of $r_0$ only and the subscript 0 symbolizes equatorial values. From (3), the sum of the magnetic and perpendicular plasma pressure in the equatorial plane does not vary along constant $r_0$. In a Hamiltonian formulation of bounce-averaged drifts, the Euler-potential $\alpha \equiv \mu_E/La$ (where $\mu_E$ denotes the geomagnetic dipole moment) serves as a magnetic-flux coordinate. The Euler potential $\beta \equiv \phi$, due to the assumption that field lines lie in constant meridian planes, serves as an azimuthal coordinate and

$$\mathbf{B} = \nabla\alpha \times \nabla\beta. \tag{4}$$

Using the Euler potential formulation (4) and the field line equation (1), the radial component of (2) can be written as a second-order ordinary differential equation in $L$ with respect to $r_0$:

$$\frac{\partial^2 L}{\partial r_0^2} = fcn\left(r_0,\ P_{\perp 0},\ P_{\parallel 0}, \frac{\partial L}{\partial r_0},\ \frac{\partial P_{\perp 0}}{\partial r_0}\right), \tag{5}$$

where the right hand side represents a function of $r_0$, the pressure distribution in the equatorial plane, and $\partial L/\partial r_0$. With a given pressure distribution and two boundary conditions, (3) and (5) can be solved to obtain $L$ and its first and second derivative and thus **B** via (4). We refer to this computation as the "force-balance solver." For the boundary conditions, we specified $L$ values at $r_0 = 2$ $R_E$ and $B_z$ values at $r_0 = 6.6$ $R_E$ and midnight from *Tsyganenko* [1989], which is parameterized by *Kp*. Although we use analytic field lines, this magnetic field model is numerical.

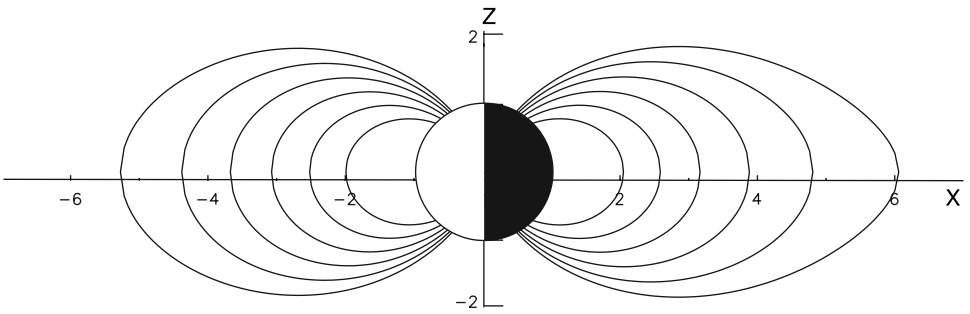


**Figure 1.** Meridional view at y = 0 of representative magnetic field lines in our model. The field lines are more stretched on the night side than on the dayside.

[6] Figure 1 shows a meridional view of representative magnetic field lines in our model. It corresponds to a simulation snapshot when there was a significant buildup of an asymmetric ring current. The figure illustrates that the field lines on the nightside are noticeably more stretched than on the dayside, which is due to the enhanced plasma pressure associated with the strong nightside ring current. Each field line corresponding to a given $r_0$ and longitude is stretched differently.

### 2.2. Electric Field

[7] For this study we apply a simple electrostatic potential function

$$\Phi_E(L,\phi) = -\frac{V_\Omega}{L} + \frac{V_0}{2}\left(\frac{L}{L^*}\right)^2 \sin\phi + \frac{\Delta V(t)}{2}\left(\frac{L}{L^*}\right)\sin\phi \tag{6}$$

that includes corotation, quiescent *Volland* [1973]-*Stern* [1974] convection, and storm-associated enhancements in the convection electric field, respectively (see *Chen et al.* [1994] for details). This electric potential function can be expressed in terms of MLT, time, and $L$. Because the magnetic field is dynamic, $L$ also depends on $r_0$ and time. Thus in addition to changes in an imposed storm-associated enhancement in the cross polar cap potential $\Delta V(t)$, the electric field intensity at a fixed location varies also because the electrostatic potential is mapped along field lines that have changed with time.

[8] We use the total cross polar cap potential from the Assimilative Model of Ionospheric Electrodynamics (AMIE) [*Richmond and Kamide*, 1988] for the 19 October 1998 storm (courtesy of G. Lu) to specify $\Delta V(t)$ in (6). The solid black curve in Figure 2 shows a trace of $V_0 + \Delta V(t)$ from 0200 UT to 1400 UT on 19 October 1998. As expected, on average the total cross polar cap potential is enhanced during the main phase of the storm. For reference the dashed curve shows the corresponding *Dst* trace. Currently, we impose the magnetospheric electric field on our model rather than try to calculate it self-consistently from particle currents and ionospheric conductivities. This is a feature that we will include in our model in the future.

### 2.3. Drift Trajectories

[9] In the equatorial plane we set up a grid of points every 0.2 $R_E$ in $r_0$ and every 5° in $\phi$. We trace the drift ($\mathbf{E} \times \mathbf{B}$ and gradient-curvature drift) backwards in time from $t = t_i + \Delta t$ to 0 for representative singly charged ions and electrons that start at the grid points. The magnetic field configuration is kept constant over a given $\Delta t$ (typically 10 min), and the time history of the fields is used. The time resolution for the non-self-consistent electric field is currently on the order of a 1 min. When the first and second invariant $M$ and $J$ are conserved, the drift equations are derived from the Hamiltonian

$$H = \left(2MB_m m_0 c^2 + m_0^2 c^4\right)^{1/2} + q\phi_E, \tag{7}$$

where $m_0$ is the rest mass, $c$ is the speed of light, $q$ is charge, and $\phi_E$ is the electric potential. An advantage of deriving the drift equations from the Hamiltonian is that the effects of the induced electric field are implicitly included. As mentioned earlier a choice of the Euler-potential $\alpha \equiv \mu_E/La$ (where $\mu_E$ denotes the geomagnetic dipole moment) serves as a magnetic-flux coordinate and the Euler potential $\beta \equiv \phi$ serves as an azimuthal coordinate. Since both of these coordinates are canonical in the Hamiltonian-Jacobi sense, it follows that the bounce-averaged particle drift rates are given by $\alpha = -(\partial H/\partial\beta)$ and $\beta = +(\partial H/\partial\alpha)$ [e.g., *Northrop*, 1963, pp. 58–59], respectively, where $H$ is the Hamiltonian function (total energy, kinetic plus potential, expressed in terms of $L$, $\phi$, $t$ = time, and the quantities regarded as adiabatically invariant). In this study we trace only equatorially mirroring particles ($J = 0$) and specify pitch angle distributions as described below.

### 2.4. Phase Space Mapping

[10] We use simulations of the drift trajectories to map phase space distributions $f$ of the particles by conserving phase space density taking account of particle loss. For

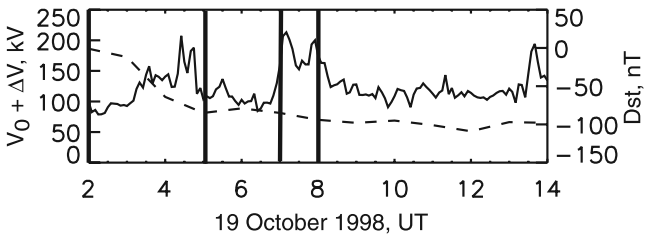


**Figure 2.** Traces of the cross polar cap potential in kV (solid curve) and *Dst* in nT (dashed curve). The black vertical lines mark respective times of interest on 19 October 1998: 0200 UT, 0500 UT, 0700 UT, and 0800 UT.

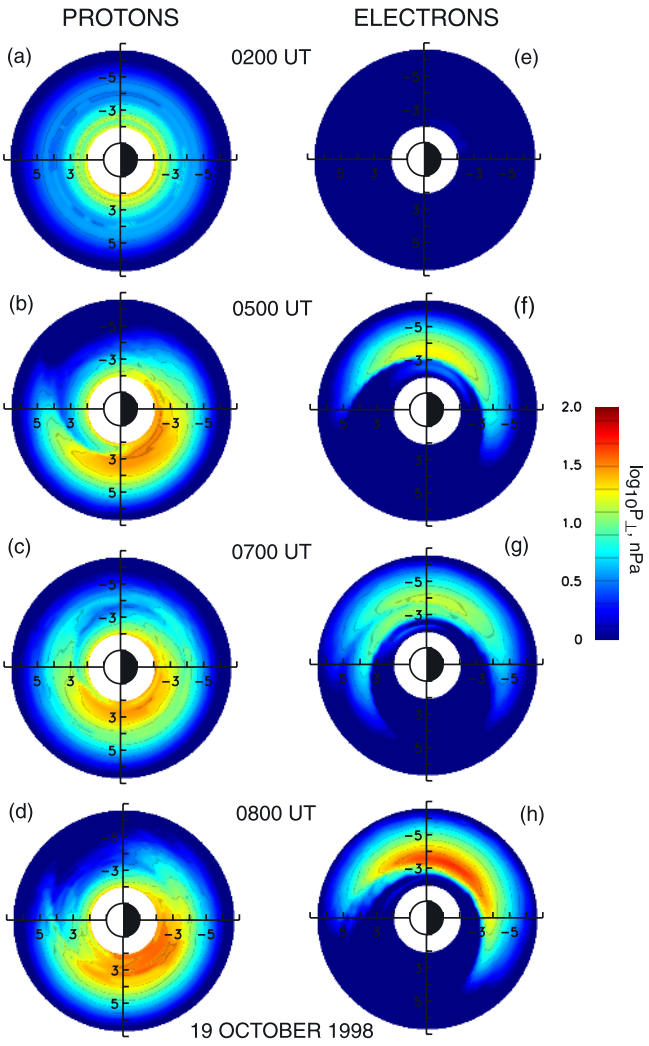


**Figure 3.** The logarithm of the simulated equatorial (proton, electron) perpendicular pressure in nPa is shown for (a, e) 0200 UT, (b, f) 0500 UT, (c, g) 0700 UT, and (d, h) 0800 UT on 19 October 1998.

example, $f$ at simulation time $t = t_i + \Delta t$ is obtained by mapping $f$ from the previous time step $t = t_i$ and attenuating it by losses. The initial conditions ($t = 0$) for protons are obtained by solving the steady-state transport equation that balances quiet time radial diffusion against charge exchange [*Chen et al.*, 1994]. For electrons, the initial conditions [*Liu et al.*, 2003] are specified by solving the steady-state transport equation that balances radial diffusion with loss due to precipitation in the limit of weak pitch angle diffusion [*Albert*, 1994]. The boundary conditions for both protons and electrons during the storm are based on fluxes obtained from the Magnetospheric Plasma Analyzer (MPA) instruments (courtesy of M. Thomsen) on LANL satellites at geosynchronous altitude. The MPA ion instrument measures total ion counts, which for this study we have treated as if it measured only the proton flux. To obtain the longitudinal variation of the boundary fluxes, we performed a least-squares fit of the *Kp*-dependent averaged LANL data of *Korth et al.* [1999] to MLT for each *Kp* value. Then, we renormalized this MLT-dependence to the LANL real time data for the associated *Kp* value to the real time data.

[11] We take account of proton charge exchange with neutral H [*Chen et al.*, 1994; 1998], the dominant collisional proton loss process. Wave-particle interactions are the dominant loss process for electrons in the inner magnetosphere. Inside the plasmasphere, we use electron lifetimes calculated by *Albert* [1994] based on pitch angle scattering by plasmaspheric hiss. Outside the plasmasphere, for electrons with a kinetic energy greater than a critical energy ($E_c$ = 2 keV), we use theoretical lifetimes against ECH waves that are proportional to $L^{-17/3}$ [*Lyons*, 1974]. For electrons outside the plasmasphere with energy less than $E_c$, we assume that their lifetimes correspond to strong pitch angle scattering [*Schulz*, 1998]. (See *Liu et al.* [2003] for details.)

[12] We assume that the equatorial phase space density $f_0$ can be expressed as

$$f_0(p, \alpha_0) = f_0(p, \alpha_0 = 90^\circ) \sin^n \alpha_0, \tag{8}$$

where $p$ is particle momentum and $\alpha_0$ is the equatorial pitch angle. This is a reasonable functional form that has been used in many observational studies of particle pitch angle distributions in the inner magnetosphere [e.g., *Garcia and Spjeldvik*, 1985; *Lui et al.*, 1990]. The equatorial perpendicular and parallel pressure components can be calculated from

$$P_{\perp 0} = 2^{3/2} m_0^{3/2} \pi B_0^{5/2} \mathrm{B}(n/2+2, 1/2) \int_0^\infty f_0 \mu^{3/2} d\mu \tag{9}$$

$$P_{\|0} = 2^{5/2} m_0^{3/2} \pi B_0^{5/2} \mathrm{B}(n/2+1, 3/2) \int_0^\infty f_0 \mu^{3/2} d\mu \tag{10}$$

where B($x$, $y$) is the Beta function. The equatorial anisotropy is $A_0 \equiv P_{\perp 0}/P_{\|0} - 1 = n/2$. We interpolate the empirical formulas of *Feshchenko and Maltsev* [2001] that approximate observed anisotropy profiles at noon and midnight of *Lui and Hamilton* [1992] to specify $A_0$ and the $n$ indices in (8) at locations of our simulation grid points in the equatorial plane. *Feshchenko and Maltsev* [2001] report that this fit is valid for quiet and moderately active times.

[13] Using (9) and (10), we calculate $P_{\perp 0}$ and $P_{\|0}$ at time intervals $\Delta t$ of 10 min. Then we compute the new magnetic field configuration that is in force balance with the plasma in the equatorial plane. This involves updating the calculation of $L$ from (5) and **B** from (4). Through this approach, we take account of the feedback of the ring current in a force-balanced magnetic field. (See *Liu et al.* [2006] for further details.)

## 3. Results

### 3.1. Simulation Results

[14] We simulated the ring current particle pressure and magnetic perturbations during the main phase of the 19 October 1998 storm. Figure 3 shows the simulated equatorial perpendicular proton (left) and electron (right) pressure at different times during the storm: 0200 UT,

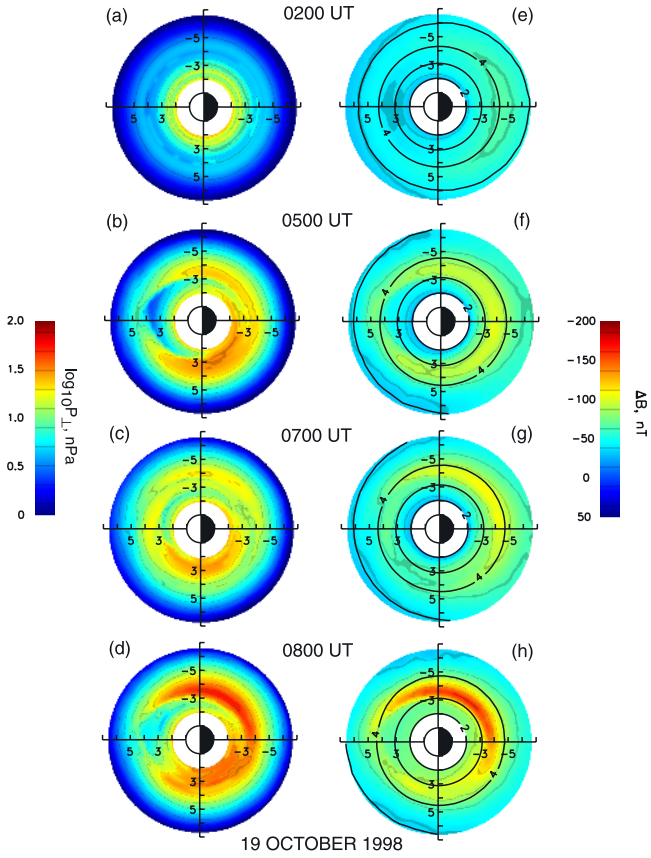


**Figure 4.** The logarithm of the simulated equatorial total perpendicular pressure in nPa is shown for (a) 0200 UT, (b) 0500 UT, (c) 0700 UT, and (d) 0800 UT on 19 October 1998. The equatorial magnetic perturbation in nT is shown for (e) 0200 UT, (f) 0500 UT, (g), 0700 UT, and (h) 0800 UT.

0500 UT, 0700 UT, and 0800 UT on 19 October 1998. For reference these times of interest are marked by the vertical thick black lines in Figure 2. In all the equatorial plots shown in this paper including Figure 3, noon is toward the left, dawn toward the top, dusk toward the bottom, and midnight is toward the right of the page. The outer boundary of the plots is at geosynchronous altitude. The color bar corresponds to the logarithm of the perpendicular pressure in units of nPa. The time of 0200 UT on 19 October 1998 corresponds to quiescent conditions (see Figures 3a and 3e). After increases in the cross-polar cap potential (see Figure 2), there were enhancements in both the equatorial proton and electron perpendicular pressure (see Figures 3b, 3c, 3d, 3f, 3g, and 3h). Enhancements in the perpendicular pressure tend to occur on the duskside for protons and on the dawnside for electrons, consistent with the corresponding direction of magnetic drift. The enhancements in the equatorial perpendicular pressure tend to occur closer to the Earth for protons (at $R_0 \equiv r_0/R_E \sim 2.5$ to 4) than for electrons ($R_0 \sim 3$ to 4.5). The total simulated equatorial perpendicular pressure, obtained by summing the proton and electron contributions, are shown in the left column of Figure 4 for different times of interest during the storm main phase. Early in the main phase of the 19 October 1998 storm (at 0500 UT) the simulated equatorial perpendicular pressure was as large as $\sim$ 30 nPa in the evening sector at $R_0 \sim 2.5$. Three hours later (at 0800 UT), the equatorial perpendicular pressure was as large was $\sim$60 nPa in the morning sector at $R_0 \sim 3.5$.

[15] The simulated equatorial magnetic perturbation in units of nT for different times of interest during the 19 October 1998 storm are displayed in the right column of Figure 4. Red on the color scale used in Figure 4 corresponds to a large magnetic depression while blue corresponds to a positive magnetic perturbation. Superimposed on the color plots of the ring current magnetic perturbations are black contours of constant $L$. At times after 0200 UT, during the storm main phase, the simulations show large longitudinally asymmetric magnetic depressions. Early in the main phase (at 0500 UT) the largest magnetic depressions was $\sim -100$ nT at $R_0 \sim 3.8$ on the nightside (see Figure 4f). Three hours later the largest depressions was $\sim -200$ nT at $R_0 \sim 3.5$ in the morning (see Figure 4h). Where the ring current was intense, the contours of the constant $L$ are more spread apart (e.g., compare Figures 4e and 4h) indicating that the magnetic field was more stretched there. Figure 5 shows the simulated azimuthal ring current density in nA/m$^2$. As expected the azimuthal current density is strongest where the largest pressure gradients occur (cf. Figures 4 and 5).

[16] It is instructive to compare the equatorial perpendicular pressure from simulations that include the feedback of the ring current (referred to as magnetically "self-consistent") and those that do not. We performed a simulation with a static axisymmetric Dungey magnetic field model in which the parameter $b$ in the field line equation (1) did not vary with MLT, $L$. or $t$. We applied the same simple electric field given by (6) over this static magnetic field model. We refer to these simulations as magnetically "non-self-consistent." The equatorial perpendicular pressure from the magnetically self-consistent and non-self-consistent simulations at different times during the 19 October 1998 storm are shown in the left and right columns of Figure 6, respectively. Comparing the plots in these columns for times after 0200 UT, it is apparent that on average the equatorial perpendicular pressure within the ring current region of $2 \leq R_0 \leq 5$ was smaller in the self-consistent simulations than in the non-self-consistent simulations. At 0500 UT (cf. Figures 6b and 6f) and 0700 UT (cf. Figures 6c and 6g), the simulated equatorial perpendicular pressure was smaller overall within the ring current region in the self-consistent simulations than in the non-self-consistent simulations. However, in the example shown for 0800 UT, there were localized regions (i.e., between 0300 MLT to 0900 MLT at $r_0 \sim 3$ to 4) where the equatorial perpendicular pressure was more intense from the self-consistent rather than non-self-consistent simulations. A similar feature was found in magnetically self-consistent simulations of the ring current for a different storm by *Zaharia et al.* [2006]. Clearly, there are significant differences between the simulated distributions of the equatorial perpendicular pressure in the ring current region during the main phase of the storm for the self-consistent and non-self-consistent runs.

[17] Such differences can be explained by the general trends of particle energization and drift rates within mag-

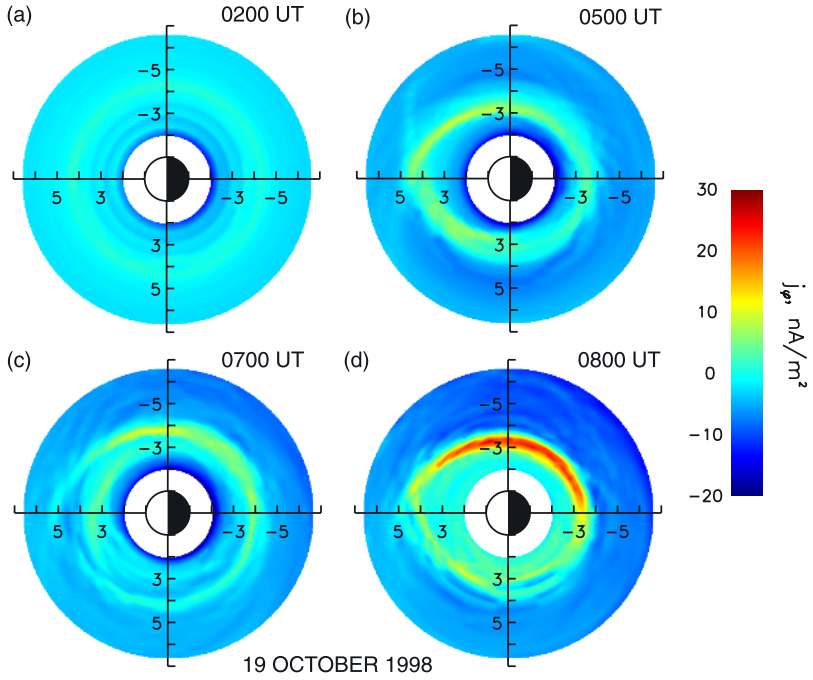


**Figure 5.** The simulated azimuthal component of the equatorial current density in nA/m$^2$ is shown for (a) 0200 UT, (b) 0500 UT, (c) 0700 UT, and (d) 0800 UT on 19 October 1998.

netic field models that do and do not take into account the feedback of the ring current. First, we consider the particle kinetic energy

$$T = (\gamma - 1)m_0c^2 \tag{11a}$$

$$= (2/(\gamma + 1))MB_m \tag{11b}$$

where $(\gamma^2 - 1) = (p/m_0c)^2 = 2MB_m/m_0c^2$ and $B_m$ is the mirror point magnetic field intensity. The kinetic energy $T$ is proportional to the mirror point magnetic intensity $B_m$ (for equatorially mirroring particles $B_m = B_0$) for constant first adiabatic invariant $M$ and where $\gamma$ is the relativistic correction. The kinetic energy for a given $M$ is smaller when the equatorial magnetic intensity is reduced by the ring current magnetic depressions. Figure 7 illustrates an example of the variation of the kinetic energy $T$ with $R_0$ for the magnetically self-consistent (solid curve) and non-self-consistent (dashed curve) for protons (Figure 7a) and electrons (Figure 7b) having $M = 5$ MeV/G, 10 MeV/G, and 15 MeV/G. For the self-consistent case, we used the model magnetic intensity corresponding to 0800 UT during the main phase of the 19 October 1998 storm. As a particle is transported inward to smaller $R_0$, the kinetic energy increases. However, comparison of the solid and dashed curves in Figures 7a and 7b illustrates that within the ring current region particles gain energy less efficiently when the feedback of the ring current is taken account. The amount of decrease of energization is larger for higher values of the first invariant $M$ as expected from (11).

[18] Not only do the ring current magnetic depressions lead to decreased efficiency of particle energization but they also affect the particle drift rates. First, we consider the **E** × **B** drift

$$v_{E/B} = E/B \tag{12a}$$

$$\propto L^2R_0. \tag{12b}$$

[19] It is not obvious from (12a) how $v_{E/B}$ will be affected by the ring current magnetic depressions. Although $B$ would be decreased, the electric intensity $E$ is also decreased in our model because the electric potential is mapped along field lines that are stretched farther apart when the feedback of the ring current is taken into account. Considering the electric potential function given by (6), we find from (12b) that $v_{E/B}$ is proportional to $L^2R_0$. Thus we would expect $v_{E/B}$ to be smaller in the ring current region with the feedback of the ring current taken into account because $L$ is reduced due to field line stretching. Figure 8a shows the variation of $v_{E/B}$ with $R_0$. The upper and lower dashed curves correspond to the magnetically non-self-consistent model at 0600 MLT and 1800 MLT, respectively. The dotted and solid curves correspond to the self-consistent model at 0600 MLT and 1800 MLT, respectively. For the self-consistent case, we used the model magnetic intensity corresponding to 0800 UT during the main phase of the 19 October 1998 storm. Indeed, comparisons of the dashed and solid curves and dashed and dotted curves in Figure 8a illustrate that the **E** × **B** drift tends to be smaller in the ring current region with the feedback of the ring current than without.

[20] Next we consider the azimuthal component of the gradient-**B** drift

$$(v_{\nabla B})_\varphi = (M/q\gamma)[(\partial B/\partial r_0)/B]. \tag{13}$$

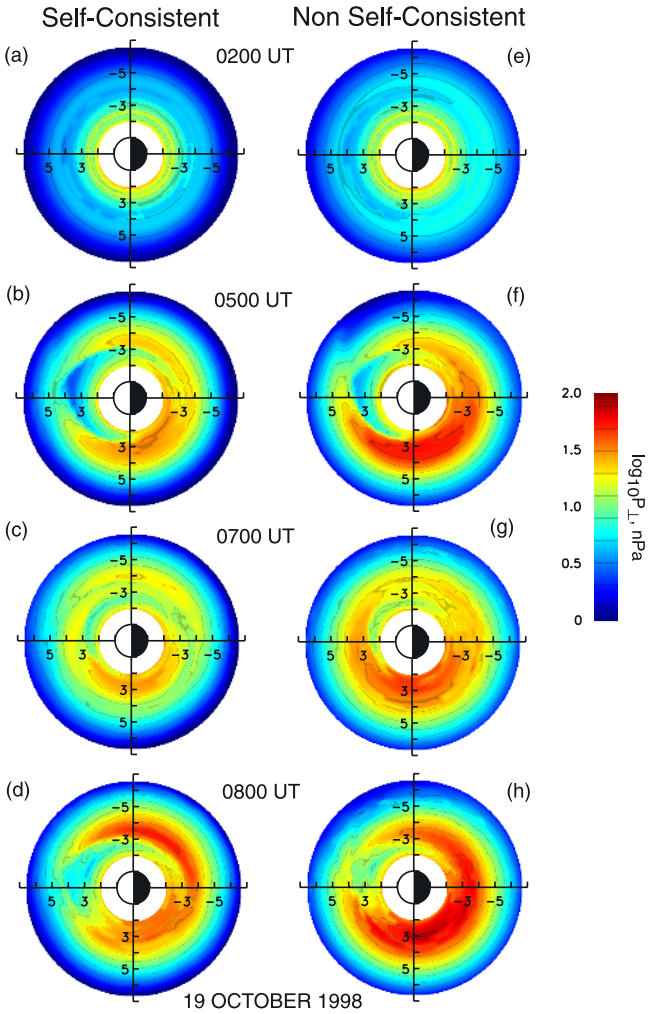


**Figure 6.** The logarithm of the simulated equatorial total perpendicular pressure in nPa (left) with and (right) without magnetic self-consistency.

The lower, middle, and upper dashed curves in Figure 8b show the variation of $(v_{\nabla B})_\varphi$ with $R_0$ for electrons with $M$ = 5 MeV/G, 10 MeV/G, and 15 MeV/G for the non-self-consistent model, respectively. The dotted and solid curves correspond to the self-consistent model at 0600 MLT and 1800 MLT, respectively. Figure 8b shows that the azimuthal component of the gradient-**B** drift tends to be significantly larger in the ring current region with the feedback of the ring current than without. The equatorial radial gradients reinforce the decreased magnetic intensity within the ring current region to increase $(v_{\nabla B})_\varphi$ (see (13)). For a given $M$ and $R_0$, the increase of the azimuthal component of the gradient-**B** drift is larger than the decrease of the **E** × **B** drift in the ring current region (cf. Figures 8a and 8b) in the magnetically self-consistent model so that there is an overall increase in the particle drift speed. More importantly, inward **E** × **B** drift is reduced and azimuthal B drift is increased. Both effects reduce earthward penetration of particles and the total ring current energization.

[21] Both the mitigation of particle energization and the enhancement of the particle drift speed are important reasons for including magnetic self-consistency in ring current simulations. Looking back at Figure 6, we can explain the overall decrease in the equatorial perpendicular pressure during the storm main phase with the magnetically self-consistent rather than non-self-consistent model by the decreased efficiency of particle energization. Comparing Figures 6d and 6h (0800 UT), the larger equatorial perpendicular pressure at 0300 MLT to 0800 MLT at $R_0$ ~3 to 4 for the self-consistent model can be explained partially by enhanced drift rates where the ring current is intense and partially by the fact that an hour before 0800 UT, there is an increase in the model cross polar cap potential (see Figure 2) that transports freshly injected particles (mainly electrons) inward. Thus it is quite conceivable that there are locations within an intense ring current where the particle pressure is larger than would have been predicted from models that did not include the feedback of the ring current. However, the expectation would be that non-self-consistent models overestimate the overall ring current particle pressure.

[22] To gauge the general overall decrease in the ring current intensity with the feedback of the ring current, we examined the ratio of the magnetic perturbations at the center of the Earth from a magnetically self-consistent $(\Delta B(0)_{sc})$ and non-self-consistent $(\Delta B(0)_{non\ sc})$ simulation for the main phase of the 19 October 1998 storm. The magnetic perturbation at the center of the Earth represents

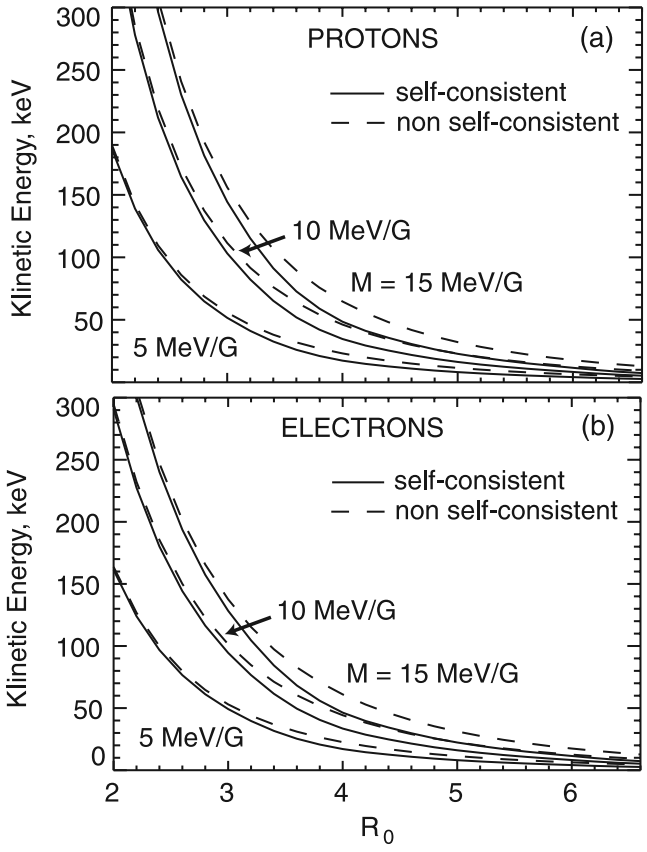


**Figure 7.** Kinetic energy versus equatorial radial distance $R_0$ for (a) protons and (b) electrons with $M$ = 5, 10, and 15 MeV/G. The dashed and solid curves correspond to simulations without and with magnetic self-consistency, respectively.

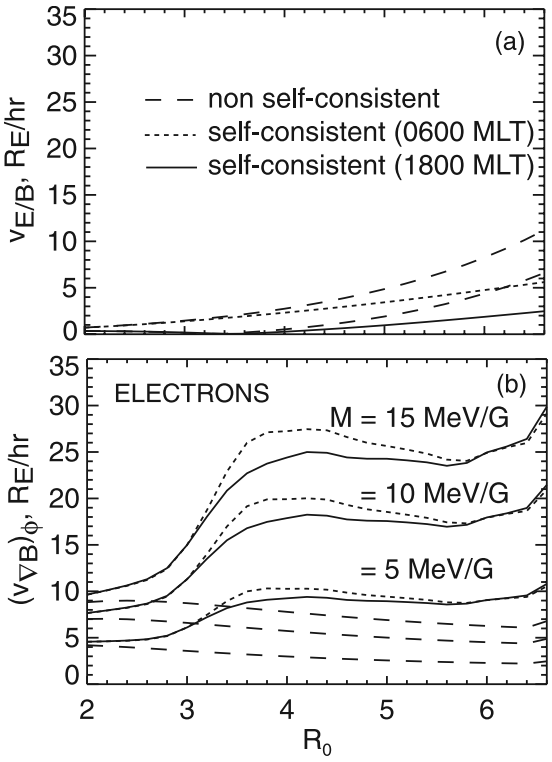


**Figure 8.** (a) The **E** × **B** drift speed in $R_E$/hr versus equatorial radial distance without (dashed upper and lower curves correspond to dawn and dusk, respectively) and with magnetic self-consistency (thick solid curve for dusk and dotted curve for dawn). (b) The azimuthal component of the electron gradient-curvature drift in $R_E$/hr versus equatorial radial distance without (dashed curves) and with magnetic self-consistency along the dusk (solid curves) and dawn (dotted curves) meridian for electrons with $M$ = 5, 10, and 15 MeV/G.

the ring current contribution to the *Dst* index. The solid curve in Figure 9 shows a trace of the ratio $\Delta B(0)_{sc}/(\Delta B(0)_{non\ sc}$. The dotted line shows the ratio of 1. The dashed curve is a trace of *Dst* (labels are on the right

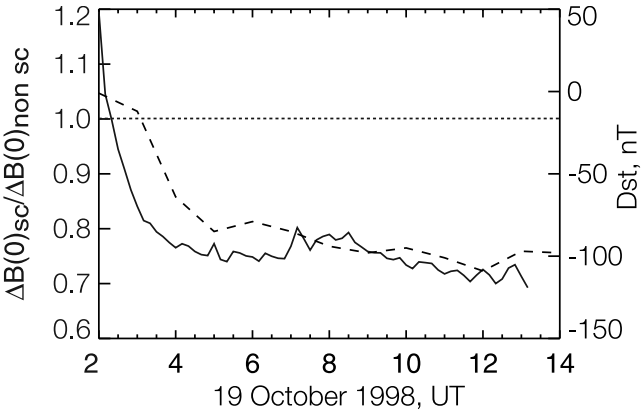


**Figure 9.** Traces of *Dst* (dashed curve) and the ratio of the magnetic perturbation at the center of the Earth with and without magnetic self-consistency (solid curve) during the main phase of the 19 October 1998 storm. The dotted line shows a ratio of 1.

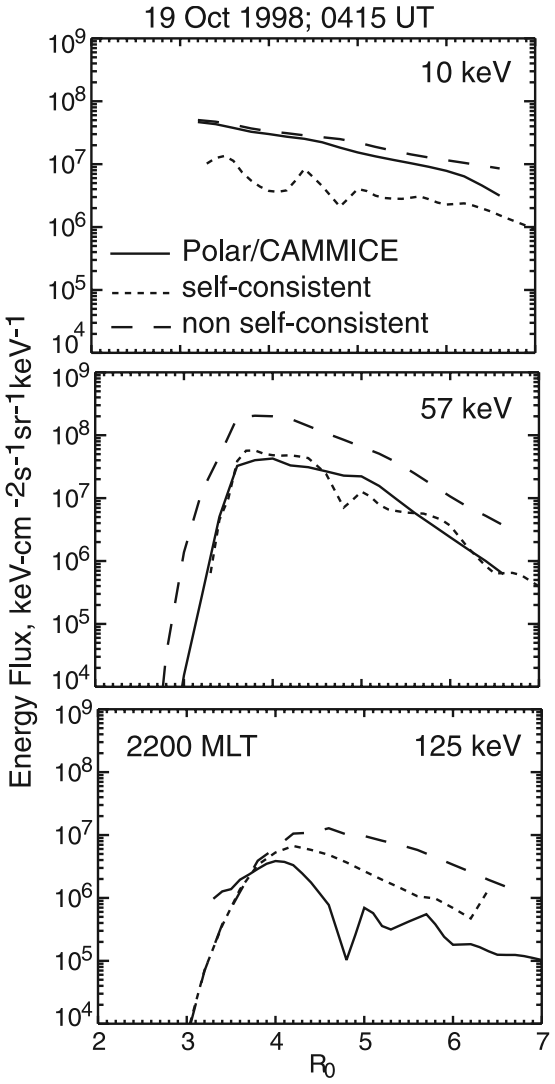


**Figure 10.** Profiles of the total ion differential energy flux from Polar/Charge and Mass Magnetospheric Ion Composition Experiment (CAMMICE) data (dotted curve) and from simulations with (solid curve) and without (dashed curve) magnetic self-consistency for energies of (a) 10 keV, (b) 57 keV, and (c) 125 keV at 0415 UT on 19 October 1998 are shown.

ordinate of the plot) to facilitate reference to the phase of the storm. Throughout the portion of the main phase shown in Figure 9 (times after ≈ 0400 UT), the magnetic perturbation at the center of the Earth in the self-consistent model is about 0.75 times that of the non-self-consistent model. Thus the average simulated ring current intensity is roughly 25% smaller with the feedback of the ring current taken into account than without for the 19 October 1998 storm.

### 3.2. Comparison of Simulations With Observations

[23] We compare our simulation results with Polar CAMMICE/MICS measurements. The Polar spacecraft was launched on 26 February 1996 into a 1.8 × 9 $R_E$ orbit (min × max geocentric distance) with a 90° inclination and an 18-hour period [*Acuna et al.*, 1995]. The Magnetospheric Ion Composition Spectrometer (MICS) that was part of the

Charge and Mass Magnetospheric Ion Composition Experiment (CAMMICE) on the Polar satellite measure all positively charged ion species ranging in mass from hydrogen to iron in the range 1–200 keV/e. The major ion species (H, He, and O) in the magnetosphere each had a low- and a high-energy channel. The data from the low- and high-energy channels may be combined into a composite spectrum in the range of 1–200 keV. A total ion channel is also recorded which counts ions irrespective of mass or charge state. Data from this channel are assumed to be protons. Details about the CAMMICE/MICS measurements can be found in the work of *Roeder et al.* [2005].

[24] The solid curves in Figure 10 are radial profiles of the total ion (or proton) differential energy flux mapped to the equator from the Polar/CAMMICE measurements at 0415 UT on 19 October 1998 at three different central energies (a) 10 keV, (b) 57 keV, and (c) 125 keV. At this early time in the main phase of the storm Polar was at premidnight at 2200 MLT. The peaks of the measured differential energy flux profiles at 57 keV and 125 keV occurred at $R_0$ of 3.8 and 4.1, respectively. The energy flux profile at 10 keV is monotonic. From the data available, the peak cannot be resolved. We note that protons with energies of 10 keV are considered to be at the low end of the ring current population, whereas energies of 57 keV and 125 keV are more representative of the ring current population.

[25] For comparison with the CAMMICE/MICS energy flux profiles, we overlay energy flux profiles from magnetically self-consistent and non-self-consistent simulations. As expected the energy flux from simulations that include magnetic feedback from the ring current is smaller than from non-self-consistent simulations. At the lowest energy shown of 10 keV, the energy flux profile from the self-consistent simulation underestimates the observed energy flux. At 57 keV and 125 keV, energies that are representative of the ring current, agreement with observations tends to be better for simulations that include the feedback of the ring current. This is especially true for the energy flux profiles at 57 keV. This good agreement with the in situ particle data is encouraging. Possible reasons for the discrepancy between the observed and model results include the simple convection electric field model used and the lack of consideration of azimuthal curvature of particles that mirror off the equator. Another source of discrepancy is that the CAMMICE data is mapped to the equator using the IGRF magnetic field that may not be sufficiently accurate during storm times. In the near future we would like to simulate particles that mirror off the equator and make simultaneous direct comparisons of the simulated magnetic field with the measured magnetic field from Polar. The simultaneous comparisons of the particle and magnetic intensity may help explain discrepancies between the model and observations.

## 4. Summary and Conclusions

[26] In this paper we report on results of a 2-D magnetically self-consistent simulation of the ring current during the storm event of 19 October 1998 storm. In our model we have imposed force balance between the equatorial magnetic field and the plasma and have included the feedback of the ring current. The self-consistent feedback between the plasma pressure and magnetic field tends to mitigate the energization associated with inward transport as the ring current forms. This is consistent with the findings of *Lemon et al.* [2004] in Rice Convection Model RCM-E simulations, of *Liu et al.* [2006] in our earlier simulations of a model storm, and of *Zaharia et al.* [2006] in a magnetic field equilibrium solver that is coupled to the Ring-Current Atmosphere (RAM) model. We have found in the ring current region that the self-consistent magnetic field reduces the $\mathbf{E} \times \mathbf{B}$ drifts but significantly enhances the azimuthal gradient-$\mathbf{B}$ drift. The net effect for the storm event that we modeled is that the drift velocity at specified $M$ and $R_0$ is enhanced due to taking account the feedback of the ring current. Both the mitigation of energization and the drift effects significantly influence ring current development.

[27] From the simulations of the 19 October 1998 storm, we find that the storm time plasma pressure and consequent magnetic perturbations are reduced overall by making the simulations magnetically self-consistent. However, especially later in the storm main phase after an intense ring current has developed, there can be places where the plasma pressure and magnetic perturbations are enhanced by making the simulation magnetically self-consistent. This situation can occur because of enhanced drift rates in regions of reduced magnetic intensity shortly after temporal enhancements in the cross polar cap potential. The magnitude of the southward magnetic perturbation at the center of the Earth, which represents the ring current contribution to the *Dst* index, is reduced by about 25% by making the simulation magnetically self-consistent. This suggests that ring current simulations that do not take account of the feedback of the ring current tend to overestimate the actual ring current intensity.

[28] We found that magnetically self-consistent simulations of proton energy flux profiles accounted for those measured by Polar/CAMMICE at energies of 57 keV and 125 keV reasonably well. This good agreement is encouraging. In the future we plan to simulate particles that mirror off the equator. In addition, we will compare simulated magnetic intensities in situ with spacecraft magnetometer data such as from Polar. This would be an important check on how well the magnetically self-consistent model can reproduce the ring current intensity. It is a more direct method than trying to account from ring current simulations the pressure-corrected *Dst** index, which is an averaged quantity that includes contributions from the tail current.

[29] **Acknowledgments.** The work of M. W. Chen, S. Liu, and L. R. Lyons was supported in part by NSF grant NSF-ATM-0202108. M. W. Chen's work was also supported by NSF grant NSF-ATM-0207160, NASA grant NAG5-12048, and by The Aerospace Corporation's Independent Research and Development Program. The work of M. Schulz was supported by NASA contract NAS5-30372, by NSF grant ATM-0201989, and by the Independent Research and Development Program of Lockheed Martin Space Systems Company. The work of J. L. Roeder was supported by Boston University under grant GC131165NGD. Computing resources were provided by the Maui High Performance Computing Center and the NASA Columbia Supercomputer.

[30] Amitava Bhattacharjee thanks Justin Kasper and another reviewer for their assistance in evaluating this paper.

## References

Acuna, M. H., K. W. Ogilvie, D. N. Baker, S. A. Curtis, D. H. Fairfield, and W. H. Mish (1995), The Global Geospace Science Program and its investigations, *Space Sci. Rev.*, *71*, 5–21.

Albert, J. M. (1994), Quasi-linear pitch angle diffusion coefficients: Retaining high harmonics, *J. Geophys. Res.*, *99*, 23,741–23,745.

Cahill, L. J. (1969), Inflation of the inner magnetosphere during a magnetic storm, *J. Geophys. Res.*, *71*, 4505–4519.

Chen, M. W., M. Schulz, and L. R. Lyons (1994), Simulations of phase space distributions of storm time proton ring current, *J. Geophys. Res.*, *99*, 5745–5759.

Chen, M. W., M. Schulz, J. L. Roeder, J. F. Fennell, and L. R. Lyons (1998), Simulations of ring current proton pitch-angle distributions, *J. Geophys. Res.*, *103*, 165–178.

Chen, M. W., M. Schulz, S. Liu, G. Lu, L. R. Lyons, M. El-Alaoui, and M. Thomsen (2005), Simulated stormtime ring-current magnetic field produced by ions and electrons, in *Inner Magnetosphere Interactions: New Perspective From Imaging*, *Geophys. Monogr. Ser.*, vol. 159, edited by J. Burch, M. Schulz, and H. Spence, pp. 237–250, AGU, Washington, D. C.

Dungey, J. W. (1961), Interplanetary magnetic field and the auroral zones, *Phys. Rev. Lett.*, *6*, 47–78.

Dungey, J. W. (1963), The structure of the exosphere or adventures in velocity space, in *Geophysics, The Earth's Environment*, edited by C. DeWitt, J. Hieblot, and A. Lebeau. pp. 503–550, Gordon and Breach, New York.

Feshchenko, E. Y., and Y. P. Maltsev (2001), Radial profile of the magnetospheric plasma pressure extracted from magnetic field data, *J. Geophys. Res.*, *106*, 21,003–21,008.

Garcia, H. A., and W. N. Spjeldvik (1985), Anisotropy characteristics of geomagnetically trapped ions, *J. Geophys. Res.*, *90*, 347–358.

Jorgensen, A. M., H. E. Spence, W. J. Hughes, and H. J. Singer (2004), A statistical study of the global structure of the ring current, *J. Geophys. Res.*, *109*, A05203, doi:10.1029/2004JA010448.

Korth, H., M. F. Thomsen, J. E. Borovsky, and D. J. McComas (1999), Plasma sheet access to geosynchronous orbit, *J. Geophys. Res.*, *104*, 25,047–25,061.

Le, G., C. T. Russell, and K. Takahashi (2004), Morphology of the ring current derived from magnetic field observations, *Ann. Geophys.*, *22*, 1267–1295.

Lemon, C., R. A. Wolf, T. W. Hill, S. Sazykin, R. W. Spiro, F. R. Toffoletto, J. Birn, and M. Hesse (2004), Magnetic storm ring current injection modeled with the Rice Convection Model and a self-consistent magnetic field, *Geophys. Res. Lett.*, *31*, L21801, doi:10.1029/2004GL020914.

Liu, S., M. W. Chen, L. R. Lyons, H. Korth, J. M. Albert, J. L. Roeder, and P. C. Anderson (2003), Contribution of convective transport to stormtime ring current electron injection J, *J. Geophys. Res.*, *108*(A10), 1372, doi:10.1029/2003JA010004.

Liu, S., M. W. Chen, M. Schulz, and L. R. Lyons (2006), Initial simulation results of storm-time ring current in a self-consistent magnetic field model, *J. Geophys. Res.*, *111*, A04225, doi:10.1029/2005JA011194.

Lui, A. T. Y. (2003), Inner magnetospheric plasma pressure distribution and its local time asymmetry, *Geophys. Res. Lett.*, *30*(16), 1846, doi:10.1029/2003GL017596.

Lui, A. T. Y., and D. C. Hamilton (1992), Radial profiles of quiet time magnetospheric parameters, *J. Geophys. Res.*, *97*, 19,325–19,332.

Lui, A. T. Y., R. W. McEntire, D. G. Sibeck, and S. M. Krimigis (1990), Recent findings on angular distributions of dayside ring current energetic ions, *J. Geophys. Res.*, *95*, 20,839–20,851.

Lyons, L. R. (1974), Electron diffusion driven by magnetospheric electrostatic waves, *J. Geophys. Res.*, *79*, 575–580.

Mead, G. D. (1964), Deformation of the geomagnetic field by the solar wind, *J. Geophys. Res.*, *69*, 1181–1195.

Northrop, T. G. (1963), *The Adiabatic Motion of Charged Particles*, Wiley Interscience, New York.

Ostapenko, A. A., and Y. P. Maltsev (2003), LT and Dst dependence of the ring current, in *Physics of Auroral Phenomena*: *Proc. XXVI Annual Seminar*, pp. 83–86, Russ. Acad. of Sci., Apatity.

Roeder, J. L., M. W. Chen, J. F. Fennell, and R. Friedel (2005), Empirical models of the low-energy plasma in the inner magnetopshere, *Space Weather*, *3*, S12B06, doi:10.1029/2005SW000161.

Richmond, A. D., and Y. Kamide (1988), Mapping electrodynamic features of the high-latitude ionosphere from localized observations: Technique, *J. Geophys. Res.*, *93*, 5471–5759.

Schulz, M. (1998), Particle drift and loss rates under strong pitch angle diffusion in Dungey's model magnetosphere, *J. Geophys. Res.*, *103*, 61–67.

Schulz, M., and M. C. McNab (1996), Source-surface modeling of planetary magnetosphere, *J. Geophys. Res.*, *101*, 5095–5118.

Stern, D. (1974), Models of the Earth's electric field, *Rep. X-602-74-159*, NASA Goddard Space Flight Cent., Greenbelt, Md.

Terada, N., T. Iyemori, M. Nosé, T. Nagai, H. Matsumoto, and T. Goka (1998), Stormtime magnetic field variations observed by the ETS-VI satellite, *Earth Planets Space*, *50*, 853–864.

Tsyganenko, N. A. (1989), A magnetospheric magnetic field model with a warped tail current sheet, *Planet. Space Sci.*, *37*, 5–20.

Tsyganenko, N. A., H. J. Singer, and J. C. Kasper (2003), Storm-time distortion of the inner magnetosphere: How severe can it get?, *J. Geophys. Res.*, *108*(A5), 1209, doi:10.1029/2002JA009808.

Turner, N. E., D. N. Baker, T. I. Pulkkinen, and R. L. McPherron (2000), Evaluation of the tail current contribution to Dst, *J. Geophys. Res.*, *105*, 5431–5440.

Volland, H. (1973), A semiempirical model of large-scale magnetospheric electric fields, *J. Geophys. Res.*, *78*, 171–180.

Wygant, J., D. Rowland, H. Singer, M. Temerin, and M. K. Hudson (1998), Experimental evidence on the role of the large spatial scale electric field in creating the ring current, *J. Geophys. Res.*, *103*, 29,527–29,544.

Zaharia, S., M. F. Thomsen, J. Birn, and M. H. Denton (2005), Effect of storm-time plasma pressure on the magnetic field in the inner magnetosphere, *Geophys. Res. Lett.*, *32*, L03102, doi:10.1029/2004GL021491.

Zaharia, S., V. K. Jordanova, M. F. Thomsen, and G. D. Reeves (2006), Self-consistent modeling of magnetic fields and plasmas in the inner magnetosphere: Application to a geomagnetic storm, *J. Geophys. Res.*, *111*, A11S14, doi:10.1029/2006JA011619.

M. W. Chen and J. L. Roeder, The Aerospace Corporation, MS M2-260, P. O. Box 92957, 2350 E. El Segundo Blvd., Los Angeles, CA 90009-2957, USA. (mchen@aero.org)

S. Liu and L. R. Lyons, Department of Atmospheric Sciences, University of California, Los Angeles, MS 71, 405 Hilgard Avenue, Los Angeles, CA 90095-1565, USA.

M. Schulz, Lockheed Martin Advanced Technology Center, 3251 Hanover Street, Palo Alto, CA 94304, USA.